Springer

Available online at https://link.springer.com/journal/42241
http://www.jhydrodynamics.com
Journal of Hydrodynamics, 2019, 31(6): 1204-1217
https://doi.org/10.1007/s42241-019-0036-y

Flow structure and unsteady fluctuation with separation over a two-dimensional backward-facing step *

Fang-fang Wang[1], Shi-qiang Wu[1], Biao Huang[2]
1. *State Key Laboratory of Hydrology-Water Resources and Hydraulic Engineering, Nanjing Hydraulic Research Institute, Nanjing 210029, China*
2. *Smart Cities Institute, Zhengzhou University, Zhengzhou 450001, China*

(Received April 16, 2017, Revised March 22, 2019, Accepted April 16, 2019, Published online April 19, 2019)

Abstract: The flow over a backward-facing step (BFS) is a typical separation and reattachment flow. Its flow structures and unsteady mechanisms are still not well explored. In this paper, the global velocity fields of a BFS are obtained by a synchronous particle image velocimetry (PIV) system with $Re_h = 5\,345$ (Reynolds number) and $E_r = 2$ (expansion ratio). Flow structures are distinguished and defined by the fraction of the negative velocity (u_{pn}). The reattachment zone (L_r) is quantitatively defined as $(u_{0.9}, u_{0.1})$ on the bottom wall. Spatial distribution of the large-scale vortices couples well with the divided flow structures and their temporal evolution presenting four stages (forming, developing, shedding and redeveloping) when travel downstream. The unsteady motions with various low frequencies are well explained by the coherent vortices and flow structures. Among the unsteady low frequency motions, the Kelvin Helmholtz (KH) vortices and the oscillation of X_r (OX) come likely from the free shear layer. The KH vortices contribute to the unsteadiness of the temporal flow, and the OX is the primary response to the vortical fluctuations.

Key words: Backward-facing step, flow structure, large-scale vortices, unsteady motion, free shear layer

Introduction

The separation and reattachment flow occurs in many configurations such as the flow in diffusers, combustors or pipes, and also in the external flow like the flow over airfoils, turbine blades, and open channels, or around buildings[1-2]. If the fluid is a mixture or in the multiphase such as the flow with pollutants, smoke or dust, the movement and the transportation of the carried particles are affected by the separation-reattachment features. Therefore, a better understanding of the separation and reattachment characteristics and the turbulent mechanisms is important both in theories and practices.

The backward-facing step (BFS) is a common geometry used in the study of the separation and reattachment flow, with rich flow phenomena though a simple geometry[3-5]. The BFS flow was widely studied, including visualizations, numerical simulations and experiments (Table 1).

In the earlier years, the flow visualizations were employed for the qualitative study such as by the streamline/pathline tracer and the high-speed photography, and more information was obtained with the development of quantitative measuring methods like the hot-wire, the hydrogen bubble and the laser Doppler velocimetry (LDV). The early achievements on the BFS flow were extensively reviewed[4, 6-8]. Some statistical parameters were summarized as the reattachment length (X_r), the time-averaged velocity, the skin friction coefficient, the pressure coefficient, the turbulent intensity, the turbulent energy, and the Reynolds stresses. These parameters provide an understanding of the mean flow characteristics.

This flow is characterized by a fixed separation point at the end of the step and goes through separation, reattachment and redevelopment in the streamwise direction. Typical flow structures are

* Project supported by the National Natural Science Foundation of China (Grant No. 51909169), The Science and Technology Support Program of Jiangsu Province (Grant No. SBK2019042181), and the Guizhou Science and Technology Cooperation Support ((2017)2865), and the International S&T Cooperation Program of China (Grant No. 2015DFA01000).
Biography: Fang-fang Wang (1988-), Male, Ph. D.,
E-mail: ffwang@nhri.cn
Corresponding author: Shi-qiang Wu, E-mail: sqwu@nhri.cn

Table 1 Previous studies of the Backward-facing step flow

Author	Fluid	Re_h	E_r	A_r^*	X_r^*	Approach
Eaton et al.[4]	-	3 000-250 000	1.07-2.00	2-166	4.90-8.20	XW/LDV/VIS
Armaly et al.[6]	Air	105-12 000	1.94	18.0	[b]7.93	LDV
Shen et al. (1984)	Water	5 900	1.90	3.2	7.00	LDV
Jovic et al. (1994)	Air	5 000	1.20	31.8	6.00±0.15	LDV
Le et al.[9]	-	5 100	1.20	4.0	6.28	DNS
Barri et al.[10]	-	[a]5 600	2.00	6.3	7.10	DNS
Kapora[11]	-	[a]9 000/6 000	2.00	6.3	8.62/8.16	DNS
Ratha and Sarkar[12]	Air	4 200	1.94	-	7.60	k-ε
Kasagi et al. (1995)	Water	6 648	1.50	20.0	6.51	PIV
Kostas et al.[13]	Water	4 660	1.02	62.0	4.80±0.20	PIV
Qi et al.[14]	Water	[a]150-6 500	2.00	36.0	[b]5.55	PIV
Wu et al.[15]	Air	3 450	1.01	96.0	4.25	PIV
Fan et al.[16]	Water	[a]500-50 000	1.50	9.1	[b]5.60	PIV
Essel et al. (2015)	Water	7 050	1.25	21.0	5.80	PIV
Present study	Water	5 345	2.00	10.0	6.08	PIV

Note: [a] Re_h is calculated by $Re = U_b h / v$, where U_b is the average velocity, [b] X_r^* is at $Re_h = 5\,345$.

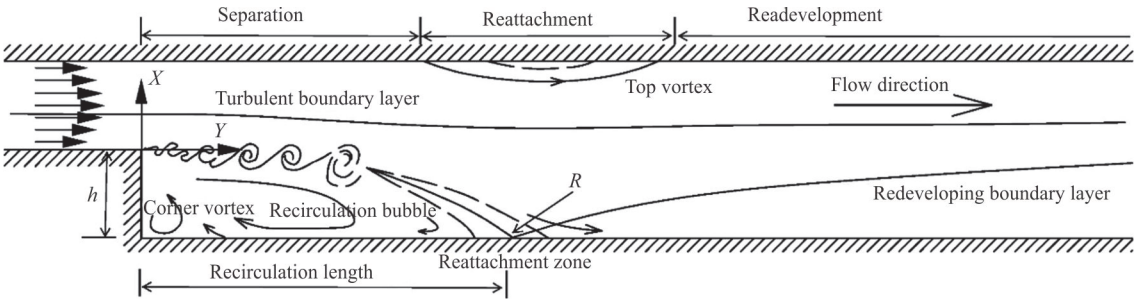

Fig. 1 Simplified representation of physical phenomena in a two-dimensional BFS flow: R is the reattachment point, h is the step height

shown in Fig. 1.

The BFS flow pattern is largely affected by the Reynolds number (Re_h), and the laminar, transitional and turbulent flow patterns, it occurs with the increase of Re_h, and the reattachment length (X_r) remains almost constant when the flow is fully developed, but before that, X_r increases in the laminar stage and then drops in the transitional stage[6]. A stable flow structure behind the step is confirmed particularly for the turbulent flow such as the recirculation bubble, the secondary vortex, the reattachment zone and the original turbulent boundary layer and the redeveloping boundary layer[17]. The flow structure is particularly produced by the special configuration and flow condition, and the quantitative predictions are needed for applications and further studies. However, the quantitative identification of the flow structure is rare in literature.

In the last decades, more detailed information for the BFS flow was made available with the successful applications of the direct numerical simulation (DNS), the large eddy simulation (LES)[9-11, 18-19] and the particle image velocimetry (PIV) measurements[5, 13-16, 20-22]. These approaches provide adequate spatio-temporal velocity and pressure information, making it possible to investigate the coherent structures and the unsteady dynamics. The quasi-periodic fluctuations of the pressure and the reattachment point were revealed, characterized by a frequency of $S_{t,h} = 0.06 - 0.098$ [7, 18, 20, 23]. This low frequency was traced to be induced by the oscillation of X_r (OX), and sometimes it was also related to the vortical shedding[20]. Beside the BFS, the OX motion was also observed in other separated configurations (the blunt plane and the separated plane). Three other low frequency phenomena were also reported in these separated flows, including the Kelvin-Helmholtz (KH) vortices, the pairing of the KH (PKH) vortices, and the flapping of the shear layer (FP), corresponding to different characteristic frequencies[18]. What is more, two distinct models were illustrated, i.e., the shear layer mode and the shedding mode by an improved delayed detached eddy simulation[23]. Three regions were suggested in the BFS flow: the shear layer region, the reattachment region and the relaxation region. And both KH and PKH phenomena occur in the shear layer

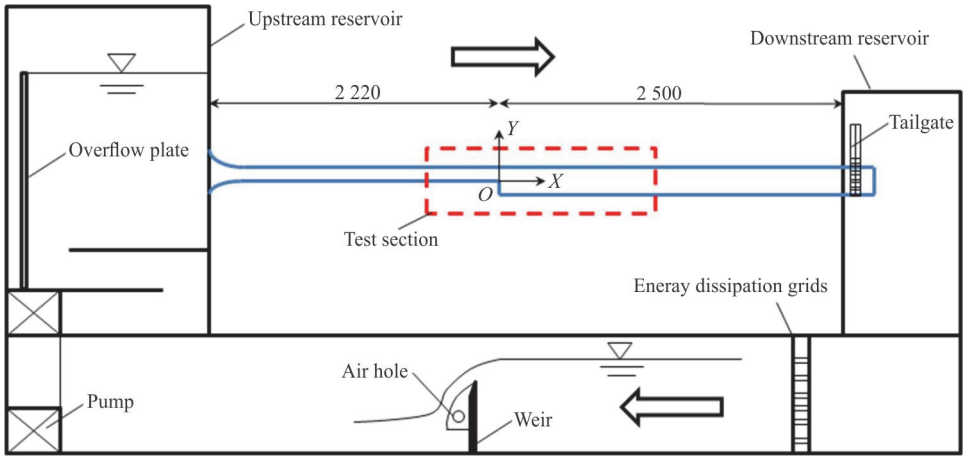

Fig. 2 (Color online) Testing apparatus (mm)

region.

Many important features of the BFS flow are not yet well understood such as the flow structures, the instability mechanisms, the coherent vortex structures, and the energy transformation or dissipation. The following issues are addressed in this paper: (1) flow structures behind the step separation, (2) the distribution and the evolution of the coherent vortical structures, (3) the unsteady motions characterized by low frequencies and (4) the correlation of the flow structures, the coherent vortices and the unsteady motions.

1. Experimental method

1.1 *Test model*

The experiment is performed in a pressured water tunnel (Fig. 2). It consists of the upstream and downstream reservoirs, the BFS test section, the tailgate, the pump and the water weir. An overflow plate is set in the upstream reservoir to ensure the stability of the water head (±1 mm). The tailgate is offset by two filter plates with uniform holes to guarantee the uniformity of the outflow.

The size of the rectangular water tunnel is 4 720 mm×500 mm×100 mm (length×width×height). A BFS ($h = 50$ mm) is set in the middle section, generating a sudden expansion (expansion ratio, $E_r = 2$) in the flow direction. The width to step height ratio, $A_r = 10$, is set to keep the bi-dimensionality[3]. The water tunnel is made of transparent PMMA (polymethyl-methacrylate) to provide a clear view for the measurements. The lengths of the upstream and downstream channels are $44h$ and $50h$, respectively. The step top corner (O) is the origin of the coordinate system, x points to the flow direction and y points to the vertical direction.

1.2 *Measurement and analysis methods*

Generally, the hardware of the PIV technique is composed of the laser, the charge coupled device (CCD) camera and the control system. For a single PIV system, the resolution of the camera and the intensity of the laser sheet are decreased with the increase of the sampling frequency and the measuring range. Previous studies show that the separation-reattachment process lasts for more than $10h$ in a BFS flow.

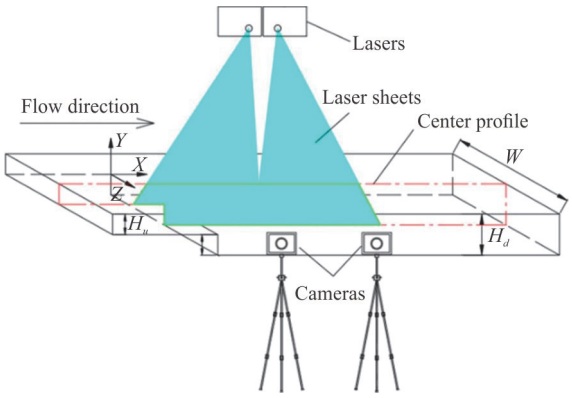

Fig. 3 (Color online) The BFS test section and the synchronous PIV system

The present study has developed a synchronous PIV apparatus that synchronizes two same PIV systems to ensure a larger range of measurement with a global view for the flow structure and a high resolution (Fig. 3). The maximum measurement range could be up to 0.6 m×0.5 m ($12h \times 10h$) with a resolution of about 10 pixels/mm. In addition, the long time and continuous data acquisition is realized to ensure enough samples for the stable statistical flow

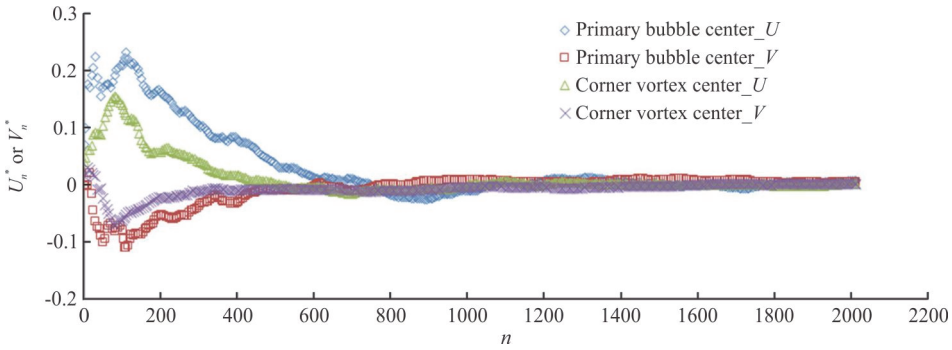

Fig. 4 (Color online) Velocity stability vs sample number

structure.

The parameters of this synchronous PIV system are as follows: (1) The laser device gives a continuous laser of 450 nanometer (power of 3 Watt, with stability $>95\%$), working with a high-speed scanning galvanometer (with response time <0.1 ms, and frequency of 0 Hz-40 Hz), (2) The resolution of the CCD camera is 2 560 pixels × 2 048 pixels, and the frame rate is 60 fps (frames per second), (3) The lasers and the CCD cameras are controlled by a synchronizer, (4) The tracer particles are glass microspheres of 20 μm in diameter and 1 000 kg/m^3- 1 050 kg/m^3 in density.

4032 instantaneous flow images are collected with a frequency of 20 Hz at the centerline profile. Thus, 2016 instantaneous velocity fields are computed with a frequency of 10 Hz. The time-averaged velocities (U, V), the fluctuating velocities (u' and v') and the non-dimensional Reynolds stress components ($(u'u')^*$, $(v'v')^*$ and $(u'v')^*$) can be, respectively, computed as

$$U=\frac{1}{ft}\sum_1^n u_i,\quad V=\frac{1}{ft}\sum_1^n v_i \tag{1}$$

$$u_i'=u_i-U,\quad v_i'=v_i-V \tag{2}$$

$$(u'u')^*=\frac{1}{n}\sum_1^n\frac{u_i'u_i'}{U_0U_0},\quad (v'v')^*=\frac{1}{n}\sum_1^n\frac{v_i'v_i'}{U_0U_0},$$

$$(u'v')^*=\frac{1}{n}\sum_1^n\frac{u_i'v_i'}{U_0U_0} \tag{3}$$

$$U_n^*=\frac{1}{n}\sum_1^n\frac{u_i}{U_0} \tag{4}$$

$$V_n^*=\frac{1}{n}\sum_1^n\frac{v_i}{U_0} \tag{5}$$

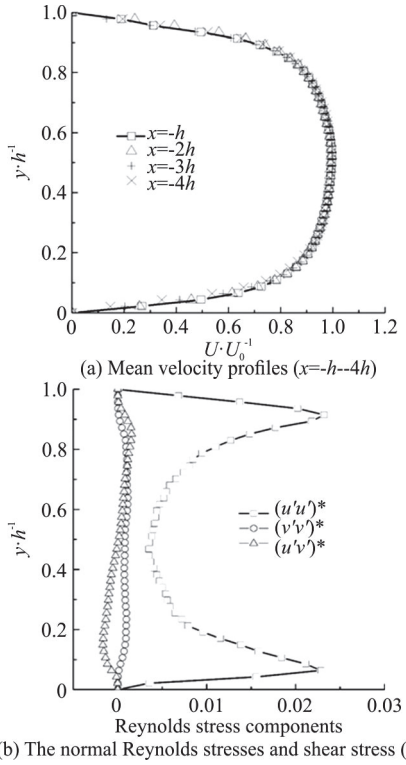

Fig. 5 Distributions of velocities and the Reynolds stress components upstream the step

The non-dimensional mean velocities U_n^* and V_n^* are stable when the sample number (n) is large enough as described by Eqs. (4), (5). The velocities at the centers of both the primary bubble and the corner vortex are calculated against n. The mean velocity $U_n^*(V_n^*)$ reaches a stable value when $n>1\,800$, indicating $n=2\,016$ in this case is enough for a stable flow structure (Fig. 4).

1.3 *Flow conditions*

A steady water head is kept with the Reynolds number $Re_h=5\,345$ based on the step height and

the maximum flow velocity at $1h$ upstream the step, where v is the kinematic viscous coefficient at 20°C. The flow conditions are summarized in Table 2.

Table 2 Flow conditions

h /10^2m	U_0 /m·s^{-1}	δ^*	E_r	A_r	Re_h
5	0.106	0.45	2:1	10	5 345

The mean velocity profiles ($x=-h$ - $-4h$) and the Reynolds stress components ($x=-4h$) of the incoming flow before the step are compared in Fig. 5. Figure 5(a) shows that the velocity distribution is uniform along the flow direction, indicating a fully developed flow. In Fig. 5(b), the distributions of $(u'u')^*$ and $(v'v')^*$ are axisymmetric, while that of $(u'v')^*$ is centrosymmetric. The value of $(u'u')^*$ is larger than the other two components, and the lines show a peak value at about $y=0.1h$ for the $(u'u')^*$ component. These results indicate the anisotropy of the turbulent flow.

2. Results and analyses

2.1 *Flow structures*

2.1.1 The instantaneous and mean flow structures

Figure 6 compares the streamlines and the velocity contours of the instantaneous and mean flows. The flow starts to diffuse with a free shear layer after passing the step corner. The mean separated streamlines turn sharply downward in the reattachment zone and impinge on the wall, where a part of the fluid in the shear layer is deflected upstream and the other part is turned downstream (Fig. 6(c)). The BFS flow develops through the separation, reattachment and redevelopment processes with a recirculation bubble behind the step and a redeveloping boundary layer beyond the reattachment zone. The large-scale vortices intensify the local unsteady turbulence.

Despite the irregular fluctuation and the interaction, the essential flow structures are well shown in the mean flow fields. The mean flow structures are regular as seen in Figs. 6(b) 6(c). The streamlines show three coherent vortices with the centers A, B and C (A is the center of the primary recirculation bubble, B is the center of the secondary vortex and C is the center of a small vortex between them). The primary recirculation bubble is the largest one with length of X_r and height of h. The secondary vortex is induced by the backflow at the step corner with the size of about $1.2h\times0.8h$. To our knowledge, the third vortex has not been reported in literature and is believed to be induced by the separation of the backflow from the bottom wall.

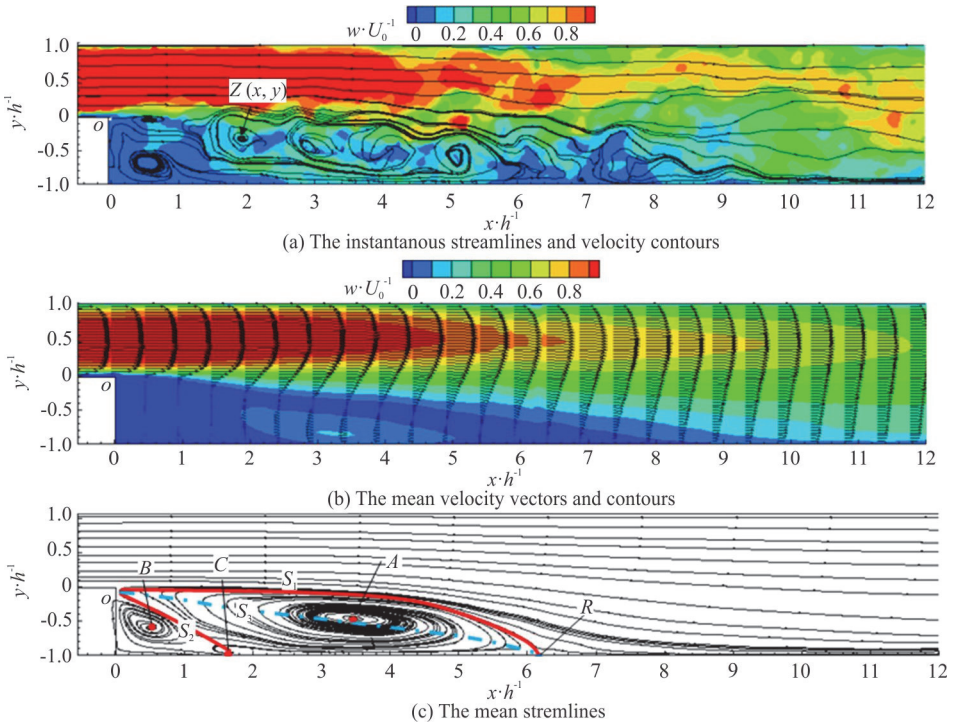

Fig. 6 (Color online)Mean and instantaneous flow structures in the x - y plane (some vectors are not shown for clarity in (b)): S_1 and S_2 are the dividing streamlines, S_3 is the centerline of the primary bubble, w is the velocity magnitude normalized by U_0. Locations $(/h)$: $O(0,0)$, $A(3.46,-0.46)$, $B(0.49,-0.59)$, $C(1.65,-0.94)$, $R(6.08,-1)$

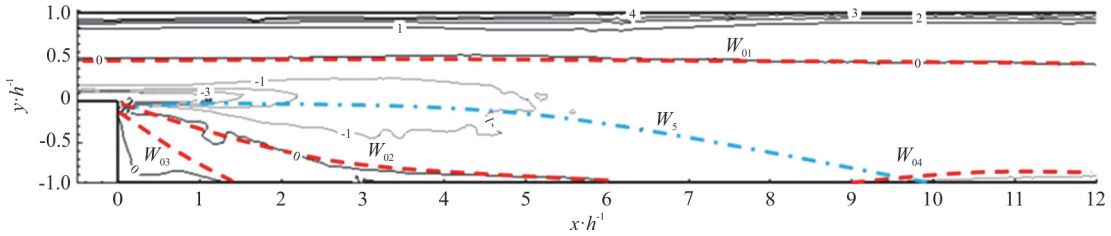

Fig. 7 (Color online) Non-dimensional mean vorticity distribution: W_{01} - W_{04} (red) are 0 contour lines and W_5 (blue) shows the developing trend

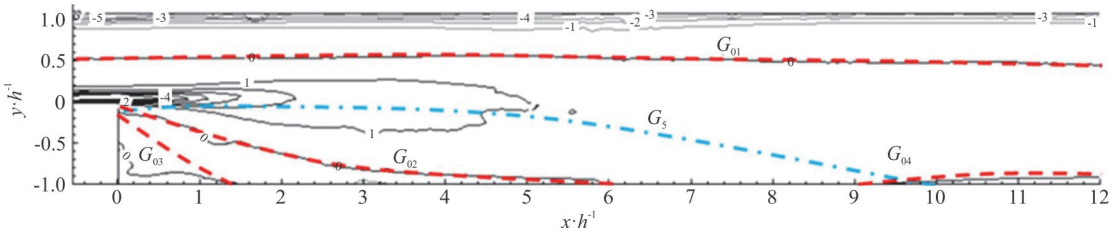

Fig. 8 (Color online) Velocity gradient distribution: G_{01} - G_{04} (red) are 0 contour lines and G_5 (blue) shows the developing trend

The primary bubble and the secondary vortex are divided by two dividing streamlines S_1 and S_2 (Fig. 6(c)). S_1 connects points O and R. This line together with the step wall and the bottom wall encompasses the main recirculation area, where the corner region (CR) is separated by another dividing streamline S_2. The CR is characterized by a counter-rotating and low-speed movement. The bubble centerline S_3 goes from O, through A to R.

The reattachment length (X_r) is an important parameter to describe these flows. In Table 1, $X_r = 6.08h$ is obtained with $Re_h = 5\,345$ and $E_r = 2$ in this study. A shorter value $X_r = 5.55h$ is obtained by Qi et al.[14] for $Re_h > 5\,400$ and $E_r = 2$, and larger values $X_r = 6.51h$, $5.6h$ are, respectively, obtained by Kasagi et al. (1995), Fan et al.[16] with the expansion ratio $E_r = 1.5$. So, the X_r value is reasonable in the current study as compared with the previous studies. The maximum backward velocity is about $0.21U_0$, which is also consistent with the previous studies [4-5, 7].

2.1.2 Flow structures

The position-based flow structures are shown in the mean vorticity and velocity gradient distributions (Figs. 7, 8). Their peak productions are located just behind the step and the contour lines grow in width with the increase of the streamwise distance. The peak contours are initially thin and spread downstream (along W_5) to a bulbous shape at $x/h = 1$ - 5, due to the active mixing behaviors of vortices[1-5]. Four zero contour lines (W_{01} - W_{04}) can distinguish the vortical behaviors, and the centerline (W_5) represents the developing direction. A negative vorticity region is surrounded by the lines W_{01} and W_{02}, which mainly enclose the clockwise rotating vortices. The line W_{03} locates in the corner region with anticlockwise vortices, and the line W_{04} indicates a new developing boundary layer near the bottom wall. The zero contour lines (G_{01} - G_{04}) and the centerline (G_5) of the velocity gradient coincide well with that of the vorticity (Fig. 8). This similarity can be explained by the definition of the vorticity, $w_z = 0.5(\partial V/\partial x - \partial U/\partial y)$, where the secondary term $\partial U/\partial y$ is just the velocity gradient. At the same time, the first term $\partial V/\partial x$ makes little or a uniform contribution to the vorticity.

The position-based flow structures are stable and independent of the mean flow fields. Together with the characteristic lines in the streamlines, they are significant for identifying the flow structures.

2.2 *Region division and reattachment zone,* L_r

2.2.1 Fraction of the part of a flow direction

The fraction of the part of a velocity direction is significant for identifying the backflows and the vortical behaviors. The fraction of the part of a flow moving downstream, γ_{puo}, was used to define the general terms for a two-dimensional separation[7]. This

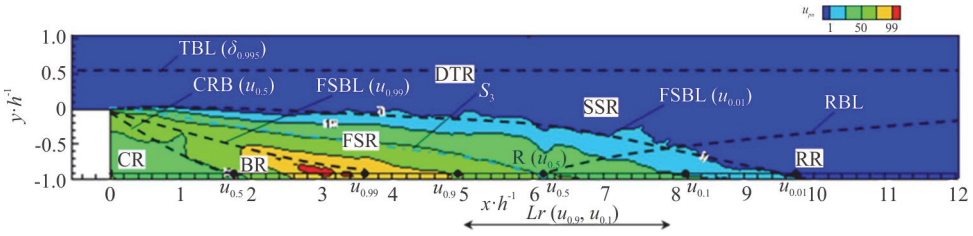

Fig. 9 (Color online) Flow region division by the two-dimensional u_{pn} distribution

parameter varies gradually from unity toward zero in the detachment zone[24]. This approach was extended to classify the separated flow over a curved step, and the flow was divided into five regions along the flow direction[25]: the attachment region, the intermittent transitory detachment region, the backflow region, the intermittent reattachment region, and the recovery region (or the redeveloping region, RR). However, this division is only one dimensional. For the current BFS study, a similar parameter, u_{pn} or v_{pn} (the fraction of the part of the negative velocity u or v), is used to define and distinguish the two-dimensional flow regions.

u_{pn} is a statistical parameter with a clear physical meaning: if $u_{pn} > 0.5$, we have the backflow, if $u_{pn} < 0.5$, we have the forward flow. $u_{0.5}$ is used to determine the reattachment position and is verified well by other methods[9, 20]. With the definition of γ_{puo}, we define: the incipient detachment (ID), $u_{pn} = 0.01$ (1% for the negative velocity), indicating the start point of appearing backflow, the intermittent transitory detachment (ITD), $u_{pn} = 0.2$ (20% for the negative velocity), the transitory detachment or reattachment (TD or TR), $u_{pn} = 0.5$, indicating the transitory detachment or reattachment position, the detachment (D), $u_{pn} = 0.9$ (90% for the negative velocity), indicating a full backflow.

The distributions of u_{pn} on the center profile are shown in Fig. 9, together with the contour lines ($u_{pn} = 0.99$, 0.9, 0.5, 0.1 and 0.01) and the characteristic structure lines (W or G). Meanwhile, the distribution of u_{pn} on the bottom wall ($y = -0.92h$) is shown in Fig. 10, where the characteristic points such as $u_{0.99}$, $u_{0.9}$, $u_{0.5}$ (or $u_{0.5'}$), $u_{0.1}$ and $u_{0.01}$ are defined.

2.2.2 Flow region division

Six flow regions are defined by the u_{pn} distribution based on the inherent flow characteristics (Fig. 9): (1) the developed turbulent region (DTR), (2) the free shear separation region (FSR), (3) the sub-shear region (SSR), (4) the corner region (CR), (5) the backflow region (BR) and (6) the redeveloping region. Sometimes, the FSR, the SSR and the BR are all called the shear region (SR).

The boundary lines of these regions are defined as follows: (1) The turbulent boundary layer TBL ($\delta_{0.995}$) is defined between the DTR and the SSR, which are coincident with the contour lines, W_{01} or G_{01}. The DTR is located above this boundary and the SSR is bellow. This line locates the interface of the influence from the upper wall to the bottom wall. (2) The FSR is favored by the large-scale vortices (Fig. 6(a)) although it is together with the SSR in the same vorticity or gradient bubble. In addition, the FSR is very sensitive to the backflow fraction u_{pn}, while the latter almost remains under 1% in the SSR. Therefore, $u_{0.01}$ contour line, the FSBL ($u_{0.01}$), is defined as the boundary of the FSR and the SSR. Coincidently, this line is fitted well with the developing trend line of the mean vorticity or velocity gradient (G_5 or W_5). (3) The lower boundary of the FSR is defined as the FSBL ($u_{0.99}$), which connects $u_{0.99}$ and the step top corner, so the lines FSBL ($u_{0.99}$) and FSBL ($u_{0.01}$) surround the FSR. These two lines have a harmonious connection between $u_{0.99} = u_{(1\text{-}0.01)}$ and $u_{pn} = 0.5$ contour line located in the middle, and this coincides well with the primary bubble centerline S_3. (4) The CR is surrounded by the step wall, the bottom wall and the CRB ($u_{0.5'}$). The flow in this region is mainly induced by the recirculation. (5) The narrow region with a higher negative velocity percentage ($u_{pn} > 0.9$) between the CR and the FSR is defined as the BR. It forms a strip heading toward the step top edge near the bottom wall. (6) A redeveloping boundary layer (RBL) develops from the reattachment zone, where some smaller local vortices re-form. These characterized lines intersect line $y = -0.92h$ with points $u_{0.01}$, $u_{0.1}$, $u_{0.5}$, $u_{0.9}$, $u_{0.99}$ and $u_{0.5'}$, respectively.

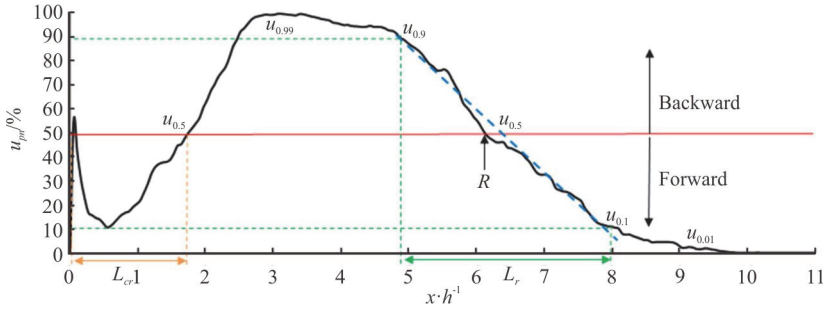

Fig. 10 (Color online) u_{pn} distribution near the bottom wall $(y = -0.92h)$

Table 3 Comparison of the locations of L_r and L_{cr} with the previous studies

Publication	Approach	Re_h	$L^*_{r\min}(h)$	$X_r^*(h)$	$L^*_{r\max}(h)$	$l_r^*(h)$	$L_{cr}^*(h)$
Eaton et al.[4]	Exp.	-	5.0	-	7.9	2.9	-
Le et al.[9]	DNS	5 100	4.8	6.28	7.9	3.1	-
Aider et al.[18]	LES	5 100	4.2	5.29	6.8	2.6	-
Aider et al.[18]	LES	5 100	4.8	5.80	7.9	3.1	-
This study	u_{pn}	5 345	$4.9(u_{0.9})$	$6.08(u_{0.5})$	$7.9(u_{0.1})$	3.0	$0\text{-}1.8(u_{0.5'})$

2.2.3 The reattachment zone

The reattachment zone $(L_r = L_{r\min} - L_{r\max})$ with a length of $l_r = L_{r\min} - L_{r\max}$ is defined as the oscillatory range of R. The location or the range of L_r is a sensitive issue, especially, for the designers, but is not well studied in literature, except some flow visualization[4] and numerical simulations[9, 18] dealing with the X_r oscillatory process. It is desirable to develop a method to predict the L_r location on the bottom wall.

In this paper, the u_{pn} approach is used to define both ends of L_r (Fig. 10). The u_{pn} fraction varies almost linearly in the reattachment zone from $x = 4.5h$ to $8.5h$ in the flow direction. Table 3 shows the results of the oscillatory X_r from previous experimental observations and numerical simulations. Their Reynolds number is 5 100, very close to 5 345 in our study. Nevertheless, the expansion ratio is $E_r = 1.2$, which is smaller than the value in this study. The oscillatory range of X_r is approximately located in $x = 4.2h\text{-}7.9h$ with a length of $l_r = 2.6h\text{-}3.1h$. Two ends of the reattachment zone, $L_{r\min}$ and $L_{r\max}$, are, respectively, fitted by $u_{0.9}$ and $u_{0.1}$ which correspond to the FSR on the bottom wall, and l_r is also computed (Fig. 10, Table 3). The fitted result is in a good agreement with previous studies, and the two ends are related with a function of $u_{0.1} = u_{(1\text{-}0.9)}$, which indicates the dependence of $L_{r\min}$ and $L_{r\max}$. In addition, $u_{0.5'}$ is defined as the dividing point of the FSR and the CR, and is also called the secondary separation point. This implies that the length of the CR, L_{cr}, is about $0h\text{-}1.8h$ in the flow direction.

2.3 *Large-scale vortex and stage division*

As Robinson[26] defined, "a vortex exists when the instantaneous streamlines mapped onto a plane normal to the vortex core exhibit a roughly circular spiral pattern, viewed from a reference frame moving with the center of the vortex core". This means the vortices should be described by the instantaneous streamlines as shown in Fig. 6(a). Therefore, the center of the instantaneous vortices shown by the streamlines is defined as $Z(x, y)$. The vortex centers of 200 instantaneous streamline fields ($n = 100\text{-}300$) with $T = tU_0/h = 21.1\text{-}63.3$) are plotted in Fig. 11. Figure 11(a) $(n = 100\text{-}200)$ and Fig. 11(b) $(n = 100\text{-}300)$ compare the influence of different number of statistical samples to the center distribution. Their similar distribution shows the independent and stable distribution in space, which also supports the position-based flow structures.

The position-based flow structures are also identified by the good coupling between the vortical distribution and the divided flow regions: (1) A large portion of centers are located along both sides of the primary bubble centerline (S_3) in the FSR. Some vortex centers are concentrated in the narrow gap $(x = 0h\text{-}2h)$ with a high shear intensity behind the

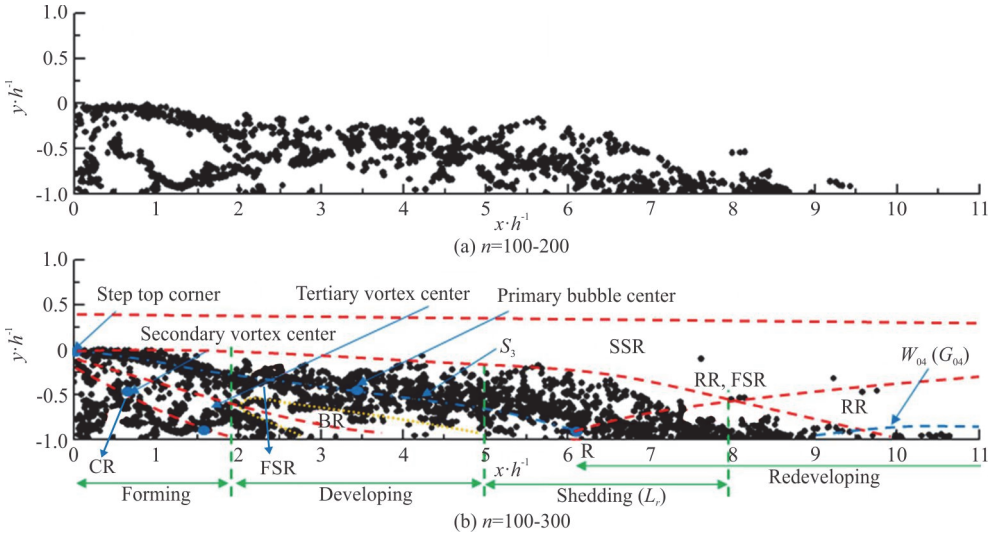

Fig. 11 (Color onlne) Distribution of the instantaneous vortical centers, with flow structures and developing stages

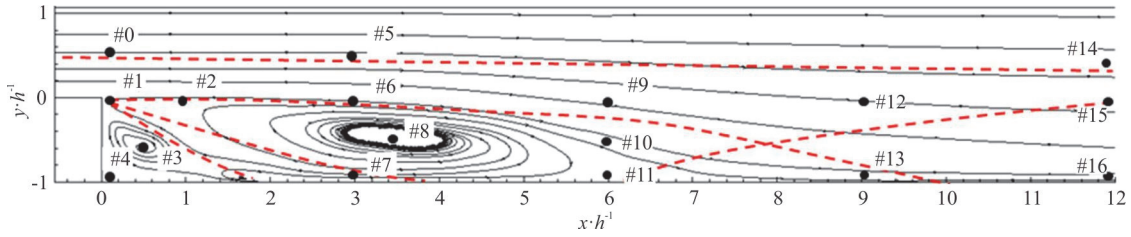

Fig. 12 (Color online) Locations of the test points: #0 ($x = 0.1h$, $y = 0.5h$), #1 ($x = 0.1h$, $y = 0h$), #2 ($x = h$, $y = 0h$), #3 ($x = 0.49h$, $y = -0.58h$), #4 ($x = 0.1h$, $y = -0.92h$), #5 ($x = 3h$, $y = 0.5h$), #6 ($x = 3h$, $y = 0h$), #7 ($x = 3h$, $y = -0.92h$), #8 ($x = 3.43h$, $y = -0.46h$), #9 ($x = 6h$, $y = 0h$), #10 ($x = 6h$, $y = -0.5h$), #11 ($x = 6h$, $y = -0.92h$), #12 ($x = 9h$, $y = 0h$), #13 ($x = 9h$, $y = -0.92h$), #14 ($x = 12h$, $y = 0.5h$), #15 ($x = 12h$, $y = 0h$), #16 ($x = 12h$, $y = -0.92h$)

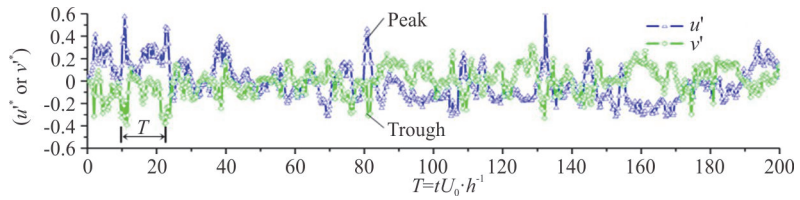

Fig. 13 (Color online) Fluctuations of turbulent velocities u' and v' at the primary bubble center ($T = 0$ - 200)

step edge and they start to branch at about $x = 2h$. (2) The vortical centers (A , B and C) of the three mean vortices are surrounded by many vortex centers. The tertiary and the secondary vortices are found to be induced by the backflow. (3) Many vortex centers are mainly located near the bottom wall in the reattachment zone and RR, and some around the redeveloping boundary layer. (4) The BR is with a high percentage of backflow, and the probability of the vortex center to be observed here is small.

These large-scale vortices play an important role in the local recirculation and the unsteady fluctuation. Vortex patterns and movements are largely dependent on their local flow conditions. Their stable and regular distribution indicates the flow structures again, corresponding well with the separation, reattachment and redevelopment processes. The vortical developing stages provide a clear identification for the large-scale vortices.

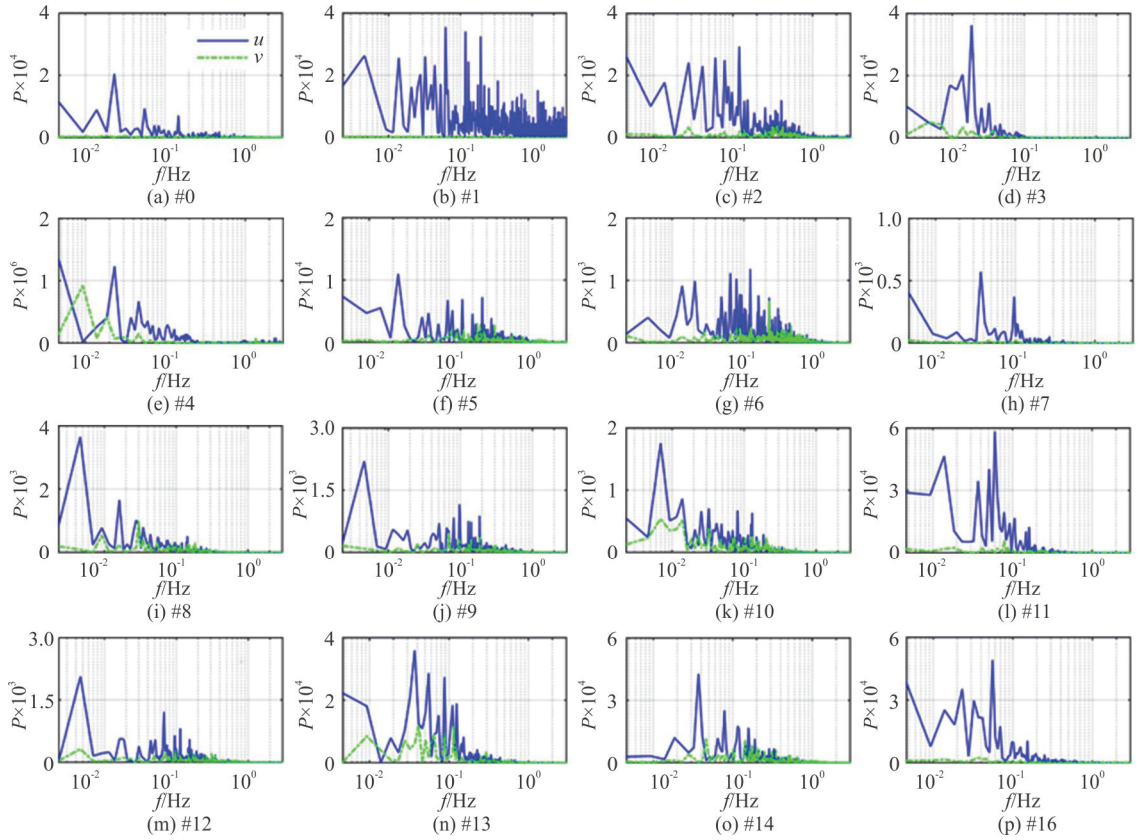

Fig. 14 (Color online) Power spectral density for velocity u' (blue solid line) and v' (green dotted line) at different positions, note: test point positions are given in Fig. 12

2.4 *Spectra analysis of velocity fluctuation*

2.4.1 Velocity fluctuation

The low frequency motions in the separated flows, including that in the present BFS configuration, were reported in literature[4, 9, 11, 18, 20-21]. Some representative test points are selected (Fig. 12) for a fast Fourier transform (FFT) analysis.

Figure 13 shows the fluctuating processes of the non-dimensional velocity u' and v' $(T = 0\text{-}200)$ at Point A. A quasi-periodical fluctuation is shown with the peak of u' and the trough of v' occurring synchronously. This fluctuation is characterized by a frequency of the Strouhal number $S_{t,h} \approx 0.08$, which is associated with the OX motion[18, 20, 22].

2.4.2 Spectral analysis and unsteady motions

Four unsteady motions as the FP, the OX, the KH and the PKH in the separated flows were reviewed by Aider et al.[18]. Multiple peaks with different $S_{t,h}$ at every test point are shown in the FFT results (Fig. 14). The predominant frequencies in the corresponding positions are summarized in Table 4. This flow is mainly predominated by low frequencies of $S_{t,h} =$ $0.005\text{-}2$, and these unsteady motions vary in different flow regions (Fig. 14, Table 4). From the overall distribution of the 17 test points, it is shown that the highest characteristic frequencies decline downstream from the step separation point, and the FSR has a wider frequency band and a stronger power spectral density. Besides these four typical flow phenomena, some LF and HF frequencies are also listed in the table. Detailed analysis based on the flow structures is as follows:

(1) In the DTR with the test points #0, #5 and #14 away from the recirculation area: There are three obvious predominant frequencies at #0, i.e., $S_{t,h} =$ 0.023 (FP), 0.056 (FP) and another relatively weaker peak with $S_{t,h} = 0.15$. The first two are affected by the FP behavior, and the last one also occurs at #5 and #14. #5 is located above the recirculation bubble with two other peaks, $S_{t,h} = 0.104$ (OX) and $S_{t,h} =$ $0.192\text{-}0.285$ (KH), which are probably originated from the FSR. 14# is away from the recirculation in the redeveloping stage $(x = 12h)$, the characteristic frequencies are a little different from those of the former two points with 0.037-0.046 (FP) and 0.078-0.12 (OX). Such a difference may contribute to the

Table 4 Representative frequency $S_{t,h}$ for velocity fluctuation (test points are depicted in Fig. 12)

Point	Location[b]	Flow phenomena with predominant frequency[c]									
		LF	FP		OX		PKH		KH		HF
Aider et al.[18]a		-	0.012	0.056	0.063	0.141	0.148	0.181	0.204	0.362	-
#0	TBL	-	**0.023**	0.056	-	-	0.150	-	-	-	-
#1	FSBL	0.005	0.014	0.033	**0.062**	0.133	-	-	**0.205**^{v}	0.250	2.000
#2	FSBL	-	**0.028**^{v}	0.043	0.078	**0.125**	0.158	0.171	0.254	0.338	0.410
#3	CR (C)	**0.005**^{v}	**0.018**	0.033	-	-	-	-	-	-	-
#4	CR	**0.009**^{v}	**0.023**	0.046	-	-	-	-	-	-	-
#5	TBL	-	**0.023**	0.057	-	0.104	0.150	-	-	0.258	-
#6	FSBL	-	0.014	0.021	0.065	**0.129**	0.158	-	**0.233**^{v}	0.300	-
#7	BR	**0.005**^{v}	-	**0.037**	0.098	-	-	-	-	-	-
#8	FSR (A)	**0.005**	0.016	**0.030**^{v}	-	-	-	-	-	-	-
#9	SSR	**0.005**	0.012	0.018	**0.07**^{v}	0.100	-	0.180	-	-	-
#10	FSBL	**0.007**	**0.014**^{v}	0.033	0.083	0.138	-	0.180	-	-	-
#11	R	-	0.014	**0.041**^{v}	**0.060**	0.108	0.150	0.163	-	-	-
#12	SSR	**0.005**	0.017	0.043	0.067	0.113	0.158	-	-	-	-
#13	RR	**0.009**	0.019	**0.030**^{v}	0.071	0.110	0.150	-	-	-	-
#14	TBL	-	**0.046**^{v}	**0.037**	0.078	0.120	0.150	-	-	-	-
#15	SSR	0.005	0.019	**0.033**	0.066	0.103	**0.163**^{v}	-	0.210	0.230	-
#16	RR	-	**0.037**^{v}	**0.056**	0.060	0.104	0.154	-	-	-	-

Note: data in bold = the maximum peak frequency (data with superscript "v" are from the "v" spectral lines, and the others are from the "u" spectral lines). [a]The data in the first row is recomputed from the data of Aider et al.[18] by $S_{t,h} = S_{t,xr} / X_r$, $X_r = 6.08h$. [b]Locations: CR(C) is the center of the secondary vortex, FSR(A) is the center of the primary bubble. Flow phenomena with predominant frequency: low frequency (LF), high frequency (HF).

recombination or regeneration of the large-scale vortices.

(2) In the CR with #3 at the secondary vortex center and #4 in the deep step corner: This region is dominant by lower frequencies, $S_{t,h} = 0.018 - 0.046$ (FP) and $S_{t,h} = 0.005 - 0.009$ (LF). The LF frequency is also found in other test points such as #1, #7-#9, #12 and #15. Similar frequency ($S_{t,h} = 0.006$) is regarded as the flapping motion in the whole shear layer[21].

(3) In the SR (including the FSR, the SSR and the BR) with test points #1, #2, #6, #8, #9-#12, where #1, #2, #6 and #11 are beside the dividing streamline S_1: These test points have different flow characteristics in the divided stages: (a) In the forming stage (#1, #2 on S_1), 1# is located behind the step with higher frequencies $S_{t,h} = 0.2 - 0.362$ (KH) and $S_{t,h} > 2.5$ (HF). It gives a good explanation for the rapidly formed vortices there. At #2 ($x = h$), the maximum $S_{t,h}$ drops to below 0.5 as the vortical size grows up and the movement e slows down. Then the KH and the PKH are more obvious in the FSR in this stage. The HF may be looked as one of the KH phenomena. (b) In the developing stage (#6 on S_1, #7 in the BR, and #8 at the center of the primary bubble), the large-scale vortices decompose and merge in this stage. Among all test points, the frequency band at #6 is the widest and the power spectral density at #8 is the strongest, indicating multi-scale and energetic motions there. Both the maximum frequencies and the power spectral density are decreased away from the FSR. In certain degree, it indicates that the FSR provides the source of unsteady motions. (c) In the shedding stage (#9 in the SSR, #10 in the FSR and #11 in L_r), #11 is mainly controlled by the FP and the OX with peaks at $S_{t,h} = 0.06$ (OX), 0.041 (FP). Another weaker frequency $S_{t,h} = 0.163$ (PKH) can be observed, with some difference from that in the developing stage. This may contribute to the shedding of the vortices. #9, #10 have similar features as #11 except for the lower frequency $S_{t,h} = 0.005 - 0.007$.

(4) In the redeveloping stage or the RR, with test points #13, #15 and #16. This region is also mainly controlled by the FP and the OX, and the KH and PKH phenomena can be seen at #15 near the new boundary layer. The near-wall test points #13 and #16 have peaks at the FP frequency, and some influence of

the OX can also be seen. This influence weakens as away from the L_r.

As is depicted above, the unsteady motions have some specific predominant frequencies in different flow regions or stages. The oscillation of X_r (OX) and the flapping (FP) seem to be common in these separated flows, nevertheless, the OX is the only phenomenon that has been observed in all configurations including the BFS, the BP and the SP[18]. Their distribution largely depends on the flow structures. The OX motion is much predominant in the separation layer but not remarkable in the CR (#3-#4) and the upstream DTR (#0), which are beyond the shear layer, unlikely to be affected by the OX. The FP motion is common in all test points, but its typical frequencies are changed from $S_{t,h}=0.023$ before the reattachment zone to $S_{t,h}=0.033$ after the reattachment zone. It generally increases in magnitude in relation to the local shear layer thickness in the flow direction, except at R. In addition, the KH instability of the shear layer is found at $S_{t,h}\approx 0.361$ ($S_{t,h}=0.204$-0.362 in this study) and its subharmonic at $S_{t,h}\approx 0.18$ ($S_{t,h}=0.148$-0.181 in this study), and it is assumed that the KH instability reduces to its subharmonic level through the vortex pairing[27]. These frequencies are believed to be related to the multi-scale vortices.

These unsteady motions have some unique features in different flow structures. It is found that the unsteady fluctuation may originate from the free shear layer and spread to the surrounding area, and they are further affected by the local flow conditions.

3. Discussions

3.1 *Flow regions and stages*

The u_{pn} approach is used for the quantitative identification and definition of the flow structures of the BFS flow. Although this method was used to define the separation points, it was not extended into the multi-dimensional problems. In this study, the divided flow regions, the vortical developing stages and the reattachment zones, all agree well with the existing knowledge. As a result, the flow structures provide a reasonable explanation for the large-scale vortex behaviors and the unsteady motions. The definition for the flow regions and stages will provide a solid foundation for investigating the separated flows.

Some limitations of this approach should be pointed out here: (1) The divided regions and stages are defined for the present BFS flow with $Re_h=5\,345$ and $E_r=2$. Actually, these flow structures largely depend on the flow pattern. When the flow is fully developed turbulent flow ($Re_h>4\,400$ [9]), it has a stable recirculation bubble behind the step. Therefore, it is suggested that this BFS flow might have the same flow structures when $Re_h>4\,400$. (2) These flow regions are based on the mean velocity fields, which is a statistical concept. (3) Four approaches were ever used to determine R on the bottom wall as follows[9]: (a) By the zero mean velocity $U=0$, (b) By the zero wall-shear stress ($\tau_w=0$, or $\partial U/\partial x=0$), (c) By the mean separated streamline ($\psi=0$), (d) By the fraction for the part of a flow direction ($\gamma_{puo}=0.5$). Among these four methods, the γ_{puo} approach, which is similar to the u_{pn} and v_{pn} in the present study, gives results with about 2% difference from those obtained by the other three approaches due to the fact that it fails to take into account the velocity magnitude. Simpson[7] noted that γ_{puo} is not a sufficient variable to describe the flow behavior since it represents only the fraction of a streamwise velocity probability distribution, but the importance of this approach was much emphasized at that time. In this study, it is shown that it plays a more superior role in identifying the backflow or the vortical motion. (4) The terms near the bottom wall are dependent on the u_{pn} values located at $y=-0.92h$ (Fig. 10). This is owing to the fact that the position of $u_{0.5}$ on this line fits best with the X_r calculated by other approaches. So, this calibration work should be firstly done to identify the flow structures.

In addition, the divided stages for the large-scale vortices are based on both the spatial distribution and the temporal vortical evolution. In other words, this result has bases both on the Euler and Lagrange concepts. It should be pointed out that the boundaries between the vortical developing stages are not so obvious and the division is not precise.

3.2 *The role of large-scale vortices in the flow structures and unsteadiness*

The large-scale vortices and the unsteady motions have various characteristics in different flow regions, as in a good agreement with the position-based flow structures. To certain extent, the inherent flow structures determine the spatial distribution for the unsteady characteristics.

These vortex structures are mainly generated in the shear layer or the turbulent boundary layer where the velocity gradient is significant. They contribute a great deal to the local unsteady fluctuation. The KH

vortices are rolled up initially and grow downstream, accelerating the mixing rate in the FSR and this influence will spread around. The large turbulence structures, with a length scale at least as large as the step height, pass through the reattachment region[7]. In this region, the flow hits on the floor where the large-scale vortices are suppressed with the deformation and the decomposition. Beyond the reattachment zone, a new redeveloping boundary layer is formed.

The unsteady motions characterized with low frequencies are closely coupled with the large-scale vortical behaviors. These motions are dependent on the flow structures, with an obvious spatial distribution.

4. Conclusions

Six flow regions are distinguished and defined based on the mean flow characteristics: (1) The developed turbulent region (DTR), (2) The free shear region (FSR), (3) The sub-shear region (SSR), (4) The corner region (CR), (5) the backflow region (BR) and (6) The redeveloping region (RR). Based on the vortical special distribution and temporal evolution, four vortical developing stages are defined: (a) the forming stage $(0 < x/h < 2)$, (b) the developing stage $(2 < x/h < 5)$, (c) The shedding stage $(5 < x/h < 8)$ and (d) The redeveloping stage $(x/h > X_r)$. In addition, the reattachment zone is quantitatively identified as $u_{0.9} < x/h < u_{0.1}$.

The coherent vortices exist and evolve in the shear layer, corresponding well with the divided flow regions and the vortical developing stages. They stem from the step top corner and interact with the local flow conditions. The BFS flow is characterized by some low frequencies $(0.005 < S_{t,h} < 2)$, showing various unsteady motions including the flapping (FP, $0.005 < S_{t,h} < 0.06$), the oscillation of X_r (OX, $0.06 < S_{t,h} < 0.14$), the Kelvin-Helmholtz vortices (KH, $0.2 < S_{t,h}$) and the pairing of the Kelvin-Helmholtz vortices (PKH, $0.14 < S_{t,h} < 0.2$). Among these motions, the KH and the OX come likely from the free shear layer. And they are believed to be the essential incarnation for the inherent unsteady fluctuations, while the other motions may be derivatives of the local vortices and the flow conditions.

References

[1] Chen L., Asai K., Nonomura T. et al. A review of Backward-Facing Step (BFS) flow mechanisms, heat transfer and control [J]. *Thermal Science and Engineering Progress*, 2018, 6: 194-216.

[2] Xu M. S., Yang X. L., Long X. P. et al. Large eddy simulation of turbulent flow structure and characteristics in an annular jet pump [J]. *Journal of Hydrodynamics*, 2017, 29(4): 702-715.

[3] Bradshaw P., Wong F. Y. F. The reattachment and relaxation of a turbulent shear layer [J]. *Journal of Fluid Mechanics*, 1972, 52: 113-135.

[4] Eaton J. K., Johnston J. P. A review of research on subsonic turbulent flow reattachment [J]. *AIAA Journal*, 1981, 19(9): 1093-1100.

[5] Ma X., Geisler R., Schröder A. Experimental investigation of separated shear flow under subharmonic perturbations over a backward-facing step [J]. *Flow Turbulence and Combustion*, 2017, 99: 71-91.

[6] Armaly B. F., Durst F. J., Pereira J. C. F. et al. Experimental and theoretical investigation of backward-facing step flow [J]. *Journal of Fluid Mechanics*, 1983, 127(6): 473-496.

[7] Simpson R. L. Review–A review of some phenomena in turbulent flow separation [J]. *Journal of Fluids Engineering*, 1981, 103(4): 520-533.

[8] Hu R. Y., Wang L., Song F. U. Review of backward-facing step flow and separation reduction [J]. *Scientia Sinica Physica, Mechanica and Astronomica*, 2015, 45(12): 124704(in chinese).

[9] Le H., Moin P., Kim J. Direct numerical simulation of turbulent flow over a backward-facing step [J]. *Journal of Fluid Mechanics*, 1997, 330: 349-374.

[10] Barri M., Khoury G. K. E., Andersson H. I. et al. DNS of backward-facing step flow with fully turbulent inflow [J]. *International Journal for Numerical Methods in Fluids*, 2010, 64(7): 777-792.

[11] Kopera M. A. Direct numerical simulation of turbulent flow over a backward-facing step [D]. Doctoral Thesis, Coventry, UK: University of Warwick, 2011.

[12] Ratha D., Sarkar A. Analysis of flow over backward facing step with transition [J]. *Frontiers of Structural and Civil Engineering*, 2015, 9(1): 71-81.

[13] Kostas J., Soria J., Chong M. Particle image velocimetry measurements of a backward-facing step flow [J]. *Experiments in Fluids*, 2002, 33(6): 838-853.

[14] Qi E. R., Huang M. H., Wei L. I. et al. An experimental study on the 2D time-average flow over a backward facing step via PIV [J]. *Journal of Experimental Mechanics*, 2006, 21(2): 225-232(in chinese).

[15] Wu Y., Ren H., Tang H. Turbulent flow over a rough backward-facing step [J]. *International Journal of Heat and Fluid Flow*, 2013, 44(4): 155-169.

[16] Fan X. J., Wu S. Q., Zhou H. et al. Investigation on the characteristics of water flow over a backward facing step under high reynolds number with particle image velocimetry [C]. *International Conference on Industrial Technology and Management Science*, Tianjin, China, 2015, 262-266.

[17] Lian Q. X. An experimental investigation of the coherent structures of the flow behind a backward facing step [J]. *Acta Mechanica Sinica*, 1993, 9(2): 129-133(in chinese).

[18] Aider J., Danet A., Lesieur M. Large-eddy simulation applied to study the influence of upstream conditions on the time-dependant and averaged characteristics of a backward-facing step flow [J]. *Journal of Turbulence*, 2007, 8: 1-30.

[19] Ding D. Y., Wu S. Q. Direct numerical simulation of turbulent flow over backward-facing at high Reynolds

numbers [J]. *Science China: Technological Sciences*, 2012, 55(11): 3213-3222.

[20] Chun S., Liu Y. Z., Sung H. J. Wall pressure fluctuations of a turbulent separated and reattaching flow affected by an unsteady wake [J]. *Experiments in Fluids*, 2004, 37(4): 531-546.

[21] Piirto M., Karvinen A., Ahlstedt H. et al. PIV measurements in square backward-facing step [J]. *Journal of Fluids Engineering*, 2007, 129(8): 984-990.

[22] Schram C., Rambaud P., Riethmuller M. L. Wavelet based eddy structure eduction from a backward facing step flow investigated using particle image velocimetry [J]. *Experiments in Fluids*, 2004, 36(2): 233-245.

[23] Hu R., Wang L., Fu S. Investigation of the coherent structures in flow behind a backward-facing step [J]. *International Journal of Numerical Methods for Heat and Fluid Flow*, 2016, 26(3-4): 1050-1068.

[24] Sandborn V. A., Liu C. Y. On turbulent boundary-layer separation [J]. *Journal of Fluid Mechanics*, 1968, 32(2): 293-304.

[25] Yin J. F., Wang R. Q., Yu S. Z. et al. LDV measurement of a turbulent separation-reattachent flow [J]. *Acta Aeronautica Et Astronautica Sinica*, 1990, 11(5): 257-261(in chinese).

[26] Robinson S. K. Coherent motions in the turbulent boundary layer [J]. *Annual Review of Fluid Mechanics*, 1991, 23(1): 601-639.

[27] Gu H., Yang J., Liu M. Study on the instability in separating–reattaching flow over a surface-mounted rib [J]. *International Journal of Computational Fluid Dynamics*, 2017, 31(2): 109-121.